Journal of Alloys and Compounds 509 (2011) 9912–9918

Contents lists available at ScienceDirect

Journal of Alloys and Compounds

journal homepage: www.elsevier.com/locate/jallcom

Effect of fuel-to-nitrate ratio on the powder characteristics of nanosized CeO_2 synthesized by mixed fuel combustion method

Haribabu Palneedi, Venu Mangam, Siddhartha Das, Karabi Das*

Department of Metallurgical and Materials Engineering, Indian Institute of Technology, Kharagpur 721302, India

ARTICLE INFO

Article history:
Received 29 June 2011
Received in revised form 26 July 2011
Accepted 28 July 2011
Available online 3 August 2011

Keywords:
Nanocrystalline materials
Cerium oxide
Mixed fuel combustion synthesis
Thermogravimetric
Raman spectroscopy

ABSTRACT

Synthesis of nanocrystalline ceria powders is carried out through the mixed fuel combustion approach by using different combinations of glycine and citric acid. The powders obtained with different fuel-to-nitrate (F/N) ratios are characterized by thermogravimetric analysis (TGA), Fourier transform infrared spectroscopy (FTIR), scanning electron microscopy (SEM), X-ray diffraction (XRD), BET surface area analysis, and Raman spectroscopy. TGA and FTIR spectroscopy studies have revealed the presence of carbonaceous species and residual volatiles in the combustion synthesized ceria powders. It is observed that the variation of fuel-to-nitrate ratio has a profound influence on the carbonaceous residues from combustion, crystallite size (11–44 nm), surface area (9–39 m^2/g) and morphology of the resultant powders. The Raman spectroscopy results on the variation of particle size with F/N ratio are consistent with the conclusions made from X-ray line broadening and BET surface area analysis.

1. Introduction

Cerium oxide is an important functional rare earth material and is widely used in a variety of applications including catalysts, fuel cells, polishing materials, ultraviolet absorbers, phosphors and oxygen sensors [1,2]. It has been observed that nanocrystalline materials exhibit superior properties compared to their microcrystalline counter parts. Nanocrystalline powders are essential as starting materials for the fabrication of nanoceramic materials. In this context, it is of significant interest to synthesize nanocrystalline cerium oxide with desired powder characteristics.

Several solution chemistry routes, such as, co-precipitation [3], combustion [4–6], hydrothermal [7] and, sol–gel [8], etc., are available for the preparation of nanocrystalline ceramic powders. Among them, combustion synthesis is a highly promising method, for producing the desired phase-pure nanosized powders in a very short time, at low cost and using simple equipment. Through the combustion method it is also possible to achieve a better control of stoichiometry and particulate properties of the final product.

Typically, the combustion process involves a self-propagating, gas producing, exothermic redox reaction between the corresponding metal nitrate and a suitable organic fuel that results in the desired products. Different organic compounds, such as urea, glycine, citric acid, and ethylene glycol, etc., have been used as fuels. Although the preparation of nanoceramic powders by combustion synthesis using a single fuel is widely studied, very few reports [9–13] are available in the literature on the use of combination of fuels. It may be noted that the mixed fuel combustion method has been reported earlier for the production of nanocrystalline ceria powders by Banerjee and Devi [13]. However, their studies were limited to the comparative evaluation of the products formed using mixed fuel and single fuel combustion synthesis.

To achieve the desired combustion reaction, the redox mixtures need to be carefully formulated. Glycine consisting of the $-NH_2$ group is a more reactive fuel than citric acid containing –OH and –COOH groups. The combustion reactions with citric acid are less violent and more controllable due to its weak exothermic nature. On the other hand, glycine with higher heat of combustion results in combustion reactions that are more violent, and difficult to control. Hence, a mixture of these two fuels with different heats of combustion and exothermicity is expected to give a good control over the exothermicity of the combustion reaction as well as the enthalpy of combustion. Purohit et al. [4] found that combustion of fuel-lean glycine–nitrate precursor yields ceria powder with improved powder characteristics. For stoichiometric and fuel-rich samples, more violent combustion reactions are observed which affected the powder properties adversely. Basu et al. [5] observed that a slightly fuel-rich composition of citrate–nitrate precursor favors a self-propagating and well controlled auto ignition reaction. Therefore, the fuel mixtures containing fuel-deficient compositions of glycine blended with stoichiometric and fuel-rich compositions of citric acid are chosen so that controlled combustion reactions resulting in powders with favorable particulate properties are achieved. It is

* Corresponding author. Tel.: +91 3222 283254; fax: +91 3222 220666.
E-mail address: karabi@metal.iitkgp.ernet.in (K. Das).

0925-8388/$ – see front matter © 2011 Elsevier B.V. All rights reserved.
doi:10.1016/j.jallcom.2011.07.087

Table 1
Fuel–nitrate compositions under study.

Sample ID	Composition	G/N ratio	C/N ratio	F/N ratio
MF1	CAN + 12.5% G + 120% CA	0.055	0.267	0.322
MF2	CAN + 25% G + 120% CA	0.110	0.267	0.377
MF3	CAN + 37.5% G + 120% CA	0.167	0.267	0.434
MF4	CAN + 12.5% G + 135% CA	0.055	0.300	0.355
MF5	CAN + 25% G + 135% CA	0.110	0.300	0.410
MF6	CAN + 37.5% G + 135% CA	0.167	0.300	0.467

CAN – ceric ammonium nitrate, G – glycine, CA – citric acid

important to emphasize here that the mixed fuel-to-nitrate ratios, used in this investigation are found to be fuel rich.

In the present work, nanosized ceria powders are synthesized using different mixed fuel compositions containing glycine and citric acid in various percentages. A systematic investigation is carried out to elucidate the influence of F/N ratio on the carbonaceous residues from combustion, crystallite size, surface area, and morphology of resultant powders. Besides that, purity of the combustion derived ceria powder is assessed by means of thermal decomposition and infrared spectroscopic studies. A comparative study is conducted on the results obtained from XRD, BET surface area analysis and Raman spectroscopy.

2. Experimental procedure

2.1. Powder synthesis

Nanocrystalline cerium oxide powders are prepared by combustion synthesis using high purity ceric ammonium nitrate (CAN) as oxidant and the mixture of glycine, and citric acid as fuel. Requisite quantities of CAN [$(NH_4)_2(Ce(NO_3)_6)$], glycine [NH_2CH_2COOH] and citric acid monohydrate [$C_6H_8O_7{\cdot}H_2O$] are mixed, in the desired molar ratios, according to the compositions given in Table 1. F/N refers to fuel-to-nitrate ratio ($F/N = M_{fuel}/M_{nitrate}$, M = molar amount of the compound). G/N and C/N refer to glycine-to-nitrate ratio and citrate-to-nitrate ratio, respectively. The redox mixture of raw materials is dissolved in a minimum amount of distilled water and stirred using a magnetic stirrer. The homogeneously mixed solution is taken in an alumina crucible, and heated at ≈200 °C in a pit furnace. During heating the solution undergoes dehydration followed by frothing and swelling which finally lead to the decomposition of the redox mixture. The auto-ignited combustion reaction is completed within a few seconds, resulting in voluminous powders. The powder samples obtained after auto-ignition are calcined at 600 °C for 3 h in a muffle furnace to remove the traces of residual reactants and left over carbonaceous matter.

Stoichiometric compositions of the redox mixtures for the combustion are calculated using the total oxidizing (O) and reducing (F) valences of the components to serve as the numerical coefficients for the stoichiometric balance, so that the equivalence ratio (O/F) is unity. This calculation is based on the thermochemical concepts used in the propellant chemistry [14]. Different compositions chosen for the synthesis of nanocrystalline cerium oxide powders and the designations used are listed in Table 1. The combustion reactions for the formation of ceria can be represented as follows:

$$MF1: (NH_4)_2[Ce(NO_3)_6] + 0.33NH_2CH_2COOH + 1.6C_6H_8O_7 \cdot H_2O + 1.96O_2 \rightarrow CeO_2 + 10.27CO_2 + 4.16N_2 + 12.83H_2O \quad (1)$$

$$MF2: (NH_4)_2[Ce(NO_3)_6] + 0.66NH_2CH_2COOH + 1.6C_6H_8O_7 \cdot H_2O + 2.7O_2 \rightarrow CeO_2 + 10.93CO_2 + 4.33N_2 + 13.67H_2O \quad (2)$$

$$MF3: (NH_4)_2[Ce(NO_3)_6] + 1NH_2CH_2COOH + 1.6C_6H_8O_7 \cdot H_2O + 3.45O_2 \rightarrow CeO_2 + 11.6CO_2 + 4.5N_2 + 14.5H_2O \quad (3)$$

$$MF4: (NH_4)_2[Ce(NO_3)_6] + 0.33NH_2CH_2COOH + 1.8C_6H_8O_7 \cdot H_2O + 2.85O_2 \rightarrow CeO_2 + 11.47CO_2 + 4.16N_2 + 13.83H_2O \quad (4)$$

$$MF5: (NH_4)_2[Ce(NO_3)_6] + 0.66NH_2CH_2COOH + 1.8C_6H_8O_7 \cdot H_2O + 3.6O_2 \rightarrow CeO_2 + 12.13CO_2 + 4.33N_2 + 14.67H_2O \quad (5)$$

$$MF6: (NH_4)_2[Ce(NO_3)_6] + 1NH_2CH_2COOH + 1.8C_6H_8O_7 \cdot H_2O + 4.35O_2 \rightarrow CeO_2 + 12.8CO_2 + 4.5N_2 + 15.5H_2O \quad (6)$$

2.2. Characterization of powders

The thermal decomposition characteristics of the as-synthesized powders are studied by thermogravimetric analysis. These studies are carried out with a PerkinElmer (Pyris Diamond) TGA system in the temperature range of 50–700 °C and at a heating rate of 10 °C/min. Fourier transform infrared spectroscopy is applied to identify the reaction intermediates, ionic species and chemical entities present in the combustion derived ceria powders. Infrared spectra of the powder samples supported on KBr pellets, are recorded in the frequency range of 400–4000 cm^{-1} using a Thermo Nicolet (Nexus 870) FTIR spectrometer. The microstructure and morphological studies of the as-prepared powders are carried out by a Zeiss (EVO 40) scanning electron microscope.

X-ray diffraction analysis of the powders is performed to know the phase formation and for estimation of the crystallite size. XRD patterns are recorded in the 2θ range 30–80° using a Bruker (D8 Advance) X-ray diffractometer, with CoKα radiation (λ = 0.179 nm). The phases formed are identified by comparison of the recorded diffraction peaks with the reference files from ICDD database. Structural broadening for the calculation of crystallite size is obtained using

$$B_{struct} = B_{obs} - B_{std} \quad (7)$$

where B_{obs} is the measured full width at half maximum (FWHM), B_{std} is the FWHM of the standard sample (corundum disc) and B_{struct} is the FWHM exclusively due to crystallite size. The crystallite size (D_{XRD}) of the powders is estimated from the X-ray line broadening of (1 1 1) peak by applying the Scherrer formula.

$$D_{XRD} = \frac{0.9\lambda}{B_{struct}\cos\theta} \quad (8)$$

The surface areas of the calcined powders are measured with a Quantachrome analyzer (ASIC9 Autosorb-1) using multipoint Brunauer–Emmett–Teller (BET) method. The particle sizes (D_{BET}) are calculated from the BET surface area (S_{BET}) values using the following relation assuming spherical particles:

$$D_{BET} = \frac{6}{\rho S_{BET}} \quad (9)$$

where ρ is the theoretical density of the powder (7.13 g/cm^3 for CeO_2). The degree or extent of agglomeration of the powder particles is evaluated via D_{BET}/D_{XRD}. Raman spectroscopy is also employed to verify the variation in particle sizes of powders from their Raman line broadening. Raman spectra of the lightly compacted powder pellets are recorded in the 300–600 cm^{-1} wave number range, with a Renishaw (RM1000B) laser Raman Microspectrometer excited at 514.5 nm using an Ar-ion laser.

3. Results and discussion

The combustion reactions are carried out by using different combinations of glycine and citric acid. Experimentally, it is observed that all the fuel–nitrate mixtures undergo combustion in a self-propagating manner with the evolution of a large volume of gases, producing a loose product. A rapid decomposition with controlled burning of the precursor materials is observed with all the samples having different F/N ratios.

To aid the comparison and for the ease of interpretation of results, the samples are grouped into two batches, based on the amount of citric acid in the fuel mixture compositions used for combustion. The first batch with 120% CA comprises of samples MF1, MF2, and MF3. The samples MF4, MF5, and MF6 having 135% CA represent the second batch.

3.1. Thermogravimetric analysis

The thermogravimetric weight loss measurements of the as-prepared ceria powders with varying F/N ratios are shown in Fig. 1.

A negligible weight loss is observed for powder samples MF3A and MF6A (A – as-synthesized). The powder sample MF4A shows the maximum weight loss. Table 2 indicates that in case of both batches, the as-formed powders with lower F/N ratios exhibit larger weight losses, indicating the presence of significant amounts of un-burnt material in them. The amount weight loss decreased with increase in the F/N ratio for samples from both batches.

From the TGA plots it is clear that, all the as-prepared powder samples obtained with different F/N ratios show a gradual weight loss until the temperature reached to 600 °C, beyond which there is very little or no decrease in weight. The weight loss up to 600 °C may

be due to the presence of un-burnt reactants, carbonaceous species and other residual matter that have remained in the as-prepared powders. As the time for which the autoignition exists is rather small, a further calcination is necessary to remove the left over residues and obtain organic free pure nanopowders. Based on the TGA results, calcination of the powders obtained after auto-ignition is carried out at 600 °C.

3.2. FTIR spectroscopy

The FTIR spectra of the as-synthesized ceria powders with different F/N ratios are presented in Fig. 2a and b. The absorption bands are more intense for samples with low F/N ratios, which have

Table 2
Thermogravimetric data for the as-prepared ceria powders.

Sample ID	F/N ratio	(%) Weight loss
MF1A	0.322	2.50
MF2A	0.377	2.32
MF3A	0.434	0.73
MF4A	0.355	3.00
MF5A	0.410	1.65
MF6A	0.467	0.97

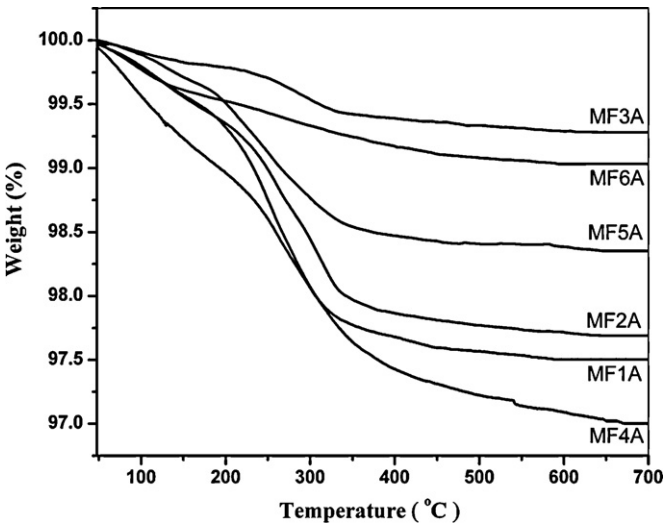

Fig. 1. TGA of as-synthesized ceria powders with different F/N ratios.

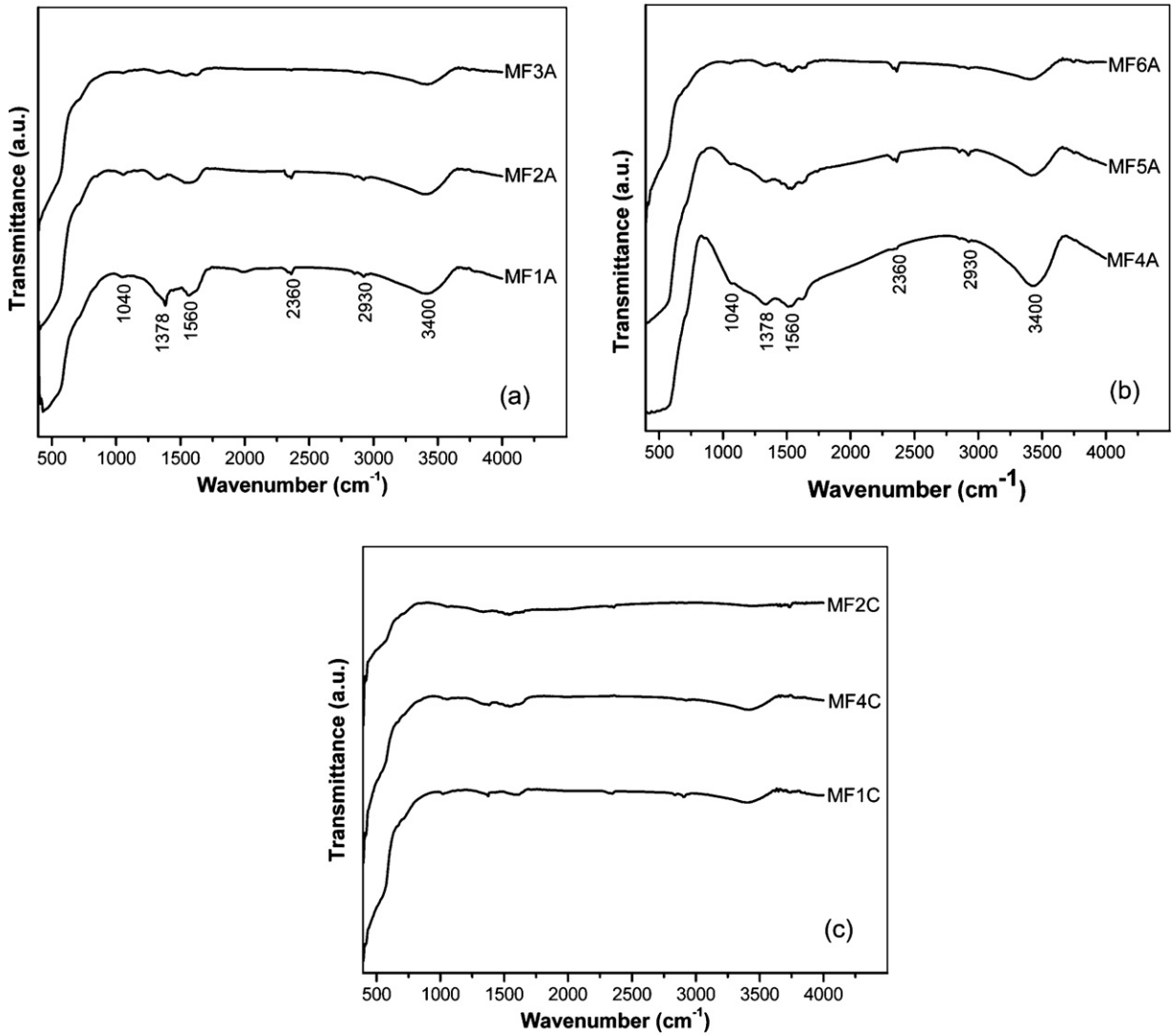

Fig. 2. FTIR spectra corresponding to (a) first and (b) second batch as-prepared, and (c) calcined ceria powders.

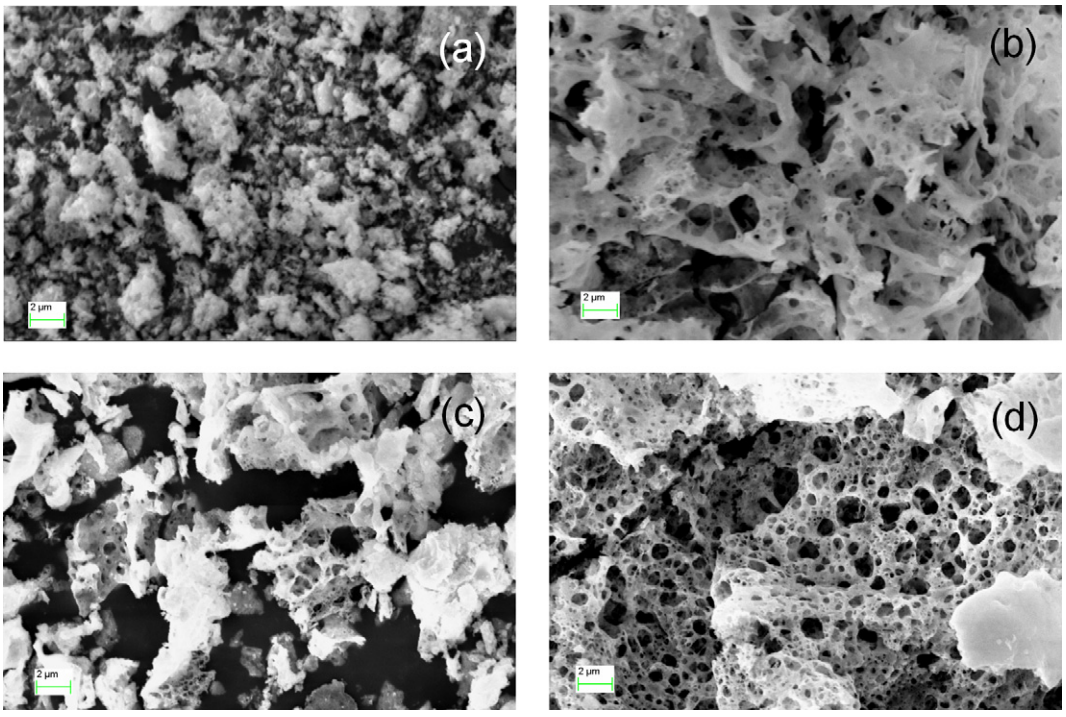

Fig. 3. SEM micrographs of the as-synthesized ceria powders obtained with F/N ratios (a) 0.322, (b) 0.434, (c) 0.355 and (d) 0.467.

shown greater weight losses during thermogravimetric measurements. The intensities of absorption peaks in the infrared spectra are reduced with increase in the F/N ratio in case of samples from both batches. This implies that more amounts of carbonaceous species and other chemical entities are present in the powders with low F/N ratios. These results, to a great extent, agree with the above TGA results as well as those reported in the literature [15]. The variations in FTIR spectral features of the as-prepared ceria powders are most probably caused by the differences in thermal decomposition behavior of their precursor materials.

All the spectra exhibit a characteristic, strong broad band below 700 cm^{-1} that represents the Ce–O stretching vibration and is typical of phonon vibration modes of ceria. This evidences that a pure ceria phase is formed directly during combustion process, which is further confirmed by the X-ray diffraction data. The vibration characteristics detected in the 1200–1700 cm^{-1} frequency region of IR spectra are attributed to the formation of carbonate species at the coordinatively unsaturated ceria surface [16]. The minor peak visible near 1040 cm^{-1} may also be related to the carbonate species. When ceria is prepared from precursors involving organic compounds, carbonates are the inevitable residual species obtained after thermal decomposition. Owing to its basic nature, CeO_2 binds with carbonates readily.

The low intensity band observed between 2340 and 2410 cm^{-1} is associated with the adsorption of linearly coordinated CO_2 molecules on the ceria surface [16]. The other weak band appearing in 2920–2960 cm^{-1} region may be assignable to C–H stretching of residual organic species resulted from the organic compounds used in the synthesis. A similar assignment has been made by Chandradass et al. [17] in their studies on Gd doped ceria nanoparticles. The reduced intensity of this band indicates that the concentration of organic moieties present in the combustion derived ceria powders is minor. All the powder samples also depict a relatively broad band centered around 3400 cm^{-1} which is caused by the O–H stretching vibration of the ceria hydroxyl groups and adsorbed moisture on the surface [18]. Residual water and hydroxyl groups are usually detected in the as-prepared powders from solution chemistry routes. The above observations reveal that the as-formed ceria powders from combustion synthesis contain some traces of carbonaceous species, residual volatiles and a further heat treatment is often needed to eliminate them.

Fig. 2c represents the FTIR spectra of some selected ceria powder samples obtained after calcination at 600 °C. The spectra of all the calcined ceria powders display similar features as that of the as-prepared ones. The intensities of absorption bands of as-prepared ceria powders are significantly decreased, upon their calcination to 600 °C. This indicates the improvement in purity of the powder. However, absorption bands due to carbonate species and hydroxyl groups are still noticeable even after calcinations. It is noteworthy here that the calcination of as-prepared samples does not necessarily represent the complete elimination of all the residual species remaining from the synthesis. And also the calcination treatment should be done at a much lower temperature in order to avoid the growth of the crystallite size of powders. Absorption of moisture during testing is also a reason for the hydroxyl bands observed, even after calcination.

3.3. Scanning electron microscopy

The SEM morphologies of the as-formed ceria powders obtained using different F/N ratios are shown in Fig. 3a–d. The microstructure of the powders exhibits three types of morphologies: (i) clusters of agglomerated particles with loose appearance (Fig. 3a); (ii) flaky aggregates with pores in their structure (Fig. 3b) and (iii) foam-like structure with high order of porosity (Fig. 3d). These highly friable, voluminous powders can be easily ground to obtain finer particles. The morphological features observed are ascribed to the inherent nature of the combustion reaction associated with evolution of large volume of gases. As the F/N ratio increases, the powder morphology changes from loose agglomerates to flaky form, in the case of first batch samples. A highly porous, continuous network-like morphology is observed for MF6A powder sample obtained with the highest F/N ratio. The SEM micrographs also reveal that

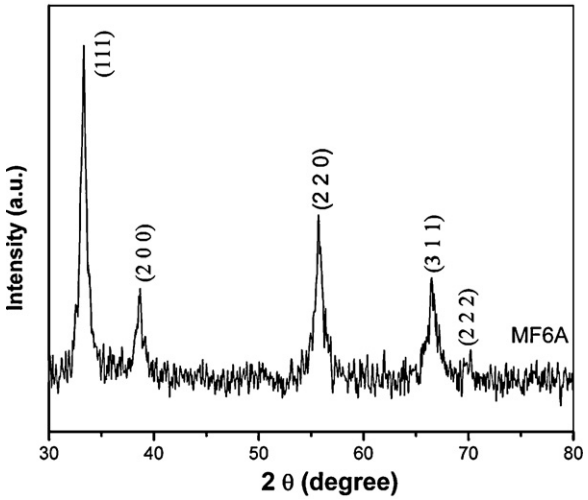

Fig. 4. XRD pattern of as-synthesized powder obtained with F/N ratio 0.467.

in each batch, the porosity of the resultant powders is increased as the fuel-to-nitrate ratio increases, due to the liberation of more amounts of gaseous products during combustion. The above observations demonstrate that the change in F/N ratio has a pronounced effect on the powder morphology and the porosity of combustion synthesized ceria powders.

3.4. X-ray diffraction measurements

The powder diffraction data of as-synthesized powders confirmed the formation of single-phase, well-crystalline ceria, with a cubic fluorite structure (ICDD file 34-0394). The XRD pattern of the as-synthesized powder obtained with F/N ratio 0.467 is shown in Fig. 4. The in situ formation of phase-pure ceria during autoignition is due to an intimate blending among the constituents and thus ascribed to the high degree of compositional homogeneity of fuel–nitrate precursor solutions.

Fig. 5 shows the variation in line broadening of (1 1 1) reflection with fuel-to-nitrate ratio. The crystallite sizes of the calcined powders, as determined from Scherrer formula, are reported in Table 3. The crystallite size is found to be in the range of 11–44 nm. The observed peak broadening of the XRD spectra gives an impression that nanosized powders are obtained from combustion synthesis. The nanocrystalline nature of these powders is explained by the substantially uniform dispersion of reactants at the molecular level in the precursor solutions.

As can be noted from Table 3, with an increase in F/N ratio, there is a decrease in crystallite size (D_{XRD}) of the ceria powders belonging to both the batches. It is also evident from the X-ray line broadening data (Fig. 5a and b) that the diffraction peaks become broader with increasing F/N ratio in each case. This observation can be explained by the increase in the number of moles of evolved gases with F/N ratio that limits the crystallite growth. The calculated amounts of gaseous products liberated in combustion reactions carried out with different fuel mixtures used in this work are also presented in Table 3. Although both the heat of combustion and the number of moles of the evolved gases, generally, increase with the increase in fuel-to-nitrate ratio, they show quite opposite effects on the crystallite size of the powders. The heat released during combustion assists in premature local partial sintering among the primary crystallites produced during combustion, there by facilitating the crystallite growth. On the other hand, the gaseous products evolved at the same time effectively dissipate the heat from the system by convection, thus hindering the growth of crystallite size. It is understood that the heat of combustion and the amount of gases released during combustion compete with each other in influencing the crystallite size of the powder product. The results obtained in the present investigation suggest that the amount of evolved gases shows a dominant effect over the heat released during combustion in controlling the crystallite size. Several other researchers have also made similar observations while working on combustion synthesis of ceria-based as well as some other metal oxide systems [15,19–21]. The trend observed in variation of crystallite size as a function of F/N ratio is further supported by the BET surface area measurements.

3.5. BET surface area analysis

The experimental specific surface areas (S_{BET}) and the calculated mean particle sizes (D_{BET}) of calcined ceria powders, corresponding to all F/N ratios are summarized in Table 3. It can be observed from the table that, as the fuel-to-nitrate ratio increases, the specific surface area of the ceria powder increases and their particle size decreases, for samples from both batches. Another important observation is that the variation of BET particle size follows the same trend as that of XRD crystallite size in response to the variation in F/N ratio. However, the particle sizes determined from surface area are higher compared to the crystallite sizes calculated using X-ray line broadening. This deviation indicates that the particles are composed of agglomerated crystallites. Table 3, gives the values of the extent or degree of agglomeration (D_{BET}/D_{XRD}) of the powder estimated for all the samples. The low values of D_{BET}/D_{XRD} obtained suggest that the ceria powders prepared by mixed fuel combustion synthesis exhibit a weaker particle agglomeration. This can be attributed to the fragmentation of combustion product and disintegration of the agglomerates due to the rapid release of gases during combustion and the simultaneous quenching of the combustion product which prevent local partial sintering and further agglomeration of particles, thereby making the powders weakly and less agglomerated. It is also observed that, there is a decrease in the extent of agglomeration with the increase in F/N ratio in case of first batch samples, while there is an increment in case of second batch samples. Calculations of particle size from specific surface area measurements usually take into account the effective adsorbed surfaces of grains or agglomerates which may be constituted of particles formed by the assembling of a bunch of crystallites and neglect the closed pores and cavities. This may also be the reason for the difference in the values of XRD crystallite size and BET particle size.

It has been reported by Djuricic and Pickering [3] that weakly agglomerated ceria powders having smaller crystallite size (<5 nm) can be obtained by a two-stage precipitation process. Further, Hirano and Kato [7] prepared ultrafine ceria powders by hydrothermal synthesis using cerium (IV) salts and urea. They have pointed out that the crystallite size decreased from 20 to 10 nm by increasing urea concentration with respect to Ce^{4+} ion. Similar observations are made in the current study also. The combustion derived nanocrystalline ceria powders show weak agglomeration and their crystallite size strongly depends on the fuel-to-nitrate ratio. Moreover, the combustion process has a good potential for large scale production of nanosized ceramic powders.

3.6. Raman spectroscopy

Raman spectroscopy is a potential tool for investigating the structural properties of nanomaterials. Raman spectra of the calcined ceria samples are depicted in Fig. 6a and b. The Raman line located at 466 cm^{-1} has been studied according to the Kosacki et al. [22] approach. As can be seen, all the Raman spectra exhibit a prominent peak at 461–466 cm^{-1} which is a characteristic of the ceria phase and corresponds to the triply degenerated F_{2g} Raman

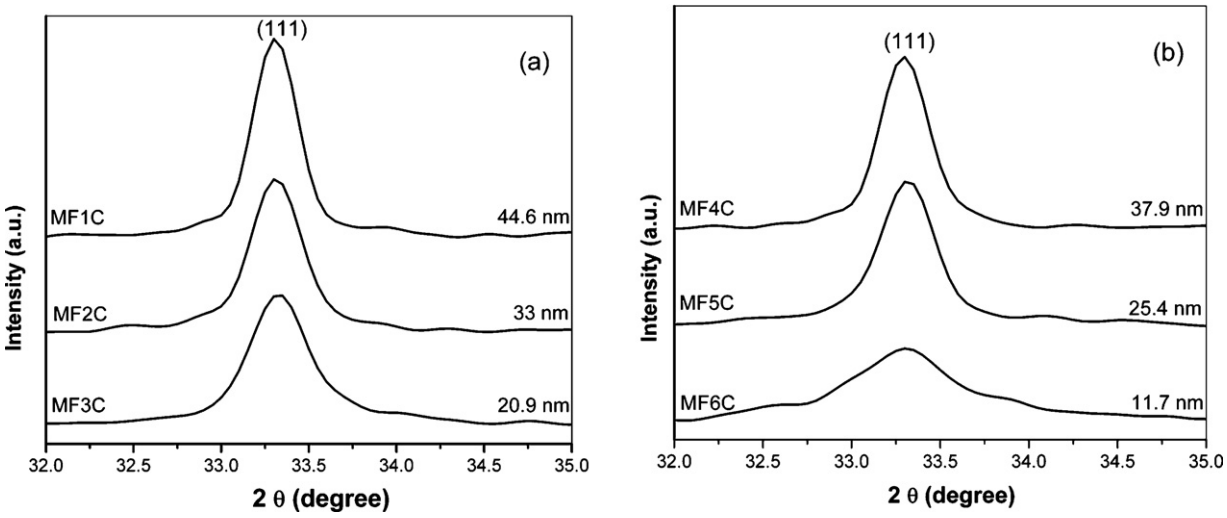

Fig. 5. X-ray line broadening for calcined ceria powder samples from (a) first and (b) second batch.

Table 3
Characteristics of the calcined ceria powders and total number of moles of gas liberated during combustion.

Sample ID	F/N ratio	Total no. of moles of gas	D_{XRD} (nm)	S_{BET} (m^2/g)	D_{BET} (nm)	Degree of agglomeration (D_{BET}/D_{XRD})	Raman line width, Γ (cm^{-1})
MF1C	0.322	27.26	44.6	12.90	65.20	1.46	9.50
MF2C	0.377	28.93	33.4	18.14	46.39	1.38	11.15
MF3C	0.434	30.60	20.9	38.94	21.61	1.03	15.28
MF4C	0.355	29.46	37.9	13.32	63.17	1.66	10.76
MF5C	0.410	31.13	25.4	17.54	47.97	1.88	13.22
MF6C	0.467	32.80	11.7	32.46	25.92	2.21	18.16

active mode of the Ce–O bond in the cubic fluorite structure. This can be viewed as a symmetric stretching mode of the [Ce–O_8] vibration unit, where the O atoms vibrate symmetrically around the Ce ions. This mode is very sensitive to any disorder in the oxygen sublattice resulting from thermal, doping, or grain-size induced effects.

There are three significant features observed, for samples from both batches, from their Raman spectra: (i) broadening of the Raman line, (ii) shift of the Raman peak position, and (iii) change in the intensity of Raman peak. The values of Raman line widths measured from their corresponding spectra are presented in Table 3. An increase in the broadening of Raman line with F/N ratio is observed from such measurements, for samples of both batches. It has been demonstrated by Kosacki et al. [22] and Weber et al. [23] that the half width at half maximum of a Raman line (Γ) is linearly proportional to the inverse of particle size or grain size (D). Hence, there shall be a decrease in the particle size with the increase in F/N ratio, which is already proven from the XRD and BET studies. The Raman bands are shifted towards lower wave numbers and their intensities are relatively decreased when the F/N ratio increases i.e., and/or as the particle size deceases. Several factors such as phonon confinement, lattice strain, inhomogeneity of the size distribution, defects, and variations in phonon relaxation with the particle size may contribute to the broadening and shifts of the

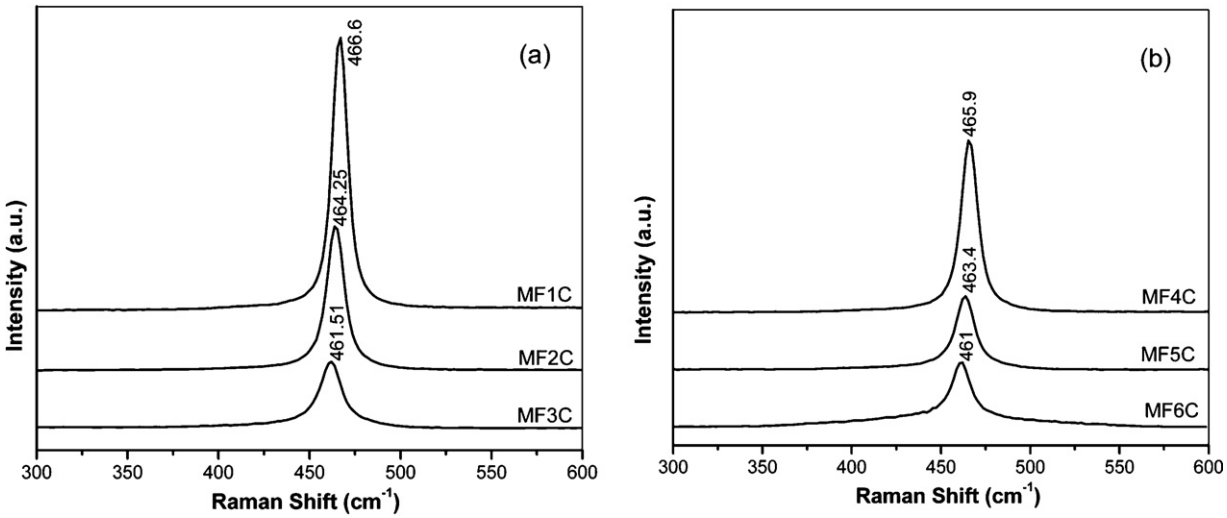

Fig. 6. Raman spectra corresponding to (a) first and (b) second batch calcined ceria powders.

F_{2g} Raman band. Size-induced variations in the vibrational amplitudes of the nearest neighbor bonds may affect the intensity of the Raman bands. The observed variations in the Raman spectral features depending on the changes in particle size of nanosized ceria corroborate the previous results [24,25]. Thus, the results of the Raman spectral studies are fully consistent with the conclusions made from the X-ray diffraction and BET surface area analysis.

4. Summary

In the current study, nanosized cerium oxide powders are successfully synthesized using the mixed fuel combustion synthesis. The FTIR spectra and XRD data confirmed the in situ formation of phase-pure cerium oxide during combustion reaction, with all mixed fuel–nitrate compositions. The weight loss observed during TGA analysis is related to the elimination of carbonaceous species and residues present in the as-synthesized ceria powders as detected from the IR spectra. It can be concluded from our experimental results that weakly and less agglomerated ceria powders with a variety of powder properties such as crystallite size of 11–44 nm and surface area of 9–39 m^2/g and also showing different morphologies are obtained through mixed fuel combustion synthesis. An explanation based on the evolution of gases during combustion reaction has been provided for the variation of powder characteristics with fuel-to-nitrate ratio. The results of the present work demonstrate that, in the mixed fuel combustion synthesis, the particle size, surface area, and morphology of the resultant powders can be broadly tuned by tailoring the fuel compositions and fuel-to-nitrate ratio.

References

[1] K.C. Patil, M.S. Hegde, T. Rattan, S.T. Aruna, Chemistry of Nanocrystalline Oxide Materials: Combustion Synthesis, Properties and Applications, World Scientific, Singapore, 2008.
[2] R.E. Kiork, D.F. Othmer, Encyclopedia of Chemistry and Technology, third ed., Wiley, New York, 1979.
[3] B. Djuricic, S. Pickering, J. Eur. Ceram. Soc. 19 (1999) 1925–1934.
[4] R.D. Purohit, B.P. Sharma, K.T. Pillai, A.K. Tyagi, Mater. Res. Bull. 36 (2001) 2711–2721.
[5] S. Basu, P.S. Devi, H.S. Maiti, J. Mater. Res. 19 (2004) 3162–3171.
[6] Venu Mangam, Karabi Das, Siddhartha Das, Mater. Chem. Phys. 120 (2010) 631–635.
[7] M. Hirano, E. Kato, J. Am. Ceram. Soc. 82 (1999) 786–788.
[8] N.B. Kirk, J.V. Wood, J. Mater. Sci. 30 (1995) 2171–2175.
[9] S.T. Aruna, K.S. Rajam, Mater. Res. Bull. 39 (2004) 157–167.
[10] M.H. Paydar, K. Tahmasebi, Mater. Chem. Phys. 109 (2008) 156–163.
[11] R. Vijayaraghavan, S. Sasikumar, Ceram. Int. 34 (2008) 1373–1379.
[12] R. Ianos, I. Lazau, C. Pacurariu, P. Barvinschi, Mater. Res. Bull. 43 (2008) 3408–3415.
[13] S. Banerjee, P.S. Devi, J. Nanopart. Res. 9 (2007) 1097–1107.
[14] S.R. Jain, K.C. Adiga, V.R. Pai Vernekar, Combust. Flame 40 (1981) 71–79.
[15] T. Mokkelbost, I. Kaus, T. Grande, M.A. Einarsrud, Chem. Mater. 16 (2004) 5489–5494.
[16] V. Bolis, G. Magnacca, G. Cerrato, C. Morterra, Thermochim. Acta 379 (2001) 147–161.
[17] J. Chandradass, B. Nam, K.H. Kim, Colloids Surf. A 348 (2009) 130–136.
[18] K. Nakamoto, Infrared and Raman Spectra of Inorganic and Coordination Compounds, second ed., Wiley, New York, 1997.
[19] B.S.B. Reddy, I. Mal, S. Tewari, K. Das, S. Das, Mater. Trans. A 38A (2007) 1786–1793.
[20] C.C. Hwang, T.Y. Wu, Mater. Sci. Eng. B 111 (2004) 197–206.
[21] J. McKittrick, L.E. Shea, C.F. Bacalski, E.J. Bosze, Displays 19 (1999) 169–172.
[22] I. Kosacki, T. Suzuki, H.U. Anderson, P. Colomban, Solid State Ionics 149 (2002) 99–105.
[23] W.H. Weber, K.C. Hass, J.R. Mcbride, Phys. Rev. B 48 (1993) 178–185.
[24] H.C. Choi, Y.M. Jung, S.B. Kim, Vib. Spectrosc. 37 (2005) 33–38.
[25] J.E. Spanier, R.D. Robinson, F. Zheng, S.W. Chan, I.P. Herman, Phys. Rev. B 64 (2001), 245407(1-8).